2024 IEEE/RSJ International Conference on Intelligent Robots and Systems (IROS)
October 14-18, 2024. Abu Dhabi, UAE

An Optimization-based Scheme for Real-time Transfer of Human Arm Motion to Robot Arm

Zhelin Yang [1†] Seongjin Bien [1] Simone Nertinger[1] Abdeldjallil Naceri[1] Sami Haddadin[1]

***Abstract*— Performing human-like motion is crucial for service humanoid robots. Real-time motion retargeting allows clear observation of the robot's pose and provides instant feedback during human demonstrator actions. This paper presents an optimization-based real-time anthropomorphic motion retargeting framework for transferring human arm motion to a robot arm. The framework is generic, applicable to both spherical-rotational-spherical (SRS) and non-SRS robot arms. We introduce the normalized normal vector of the arm plane as an anthropomorphic criterion within our framework. The method is validated on a service humanoid robot, with both static and dynamic evaluations. The statistical analysis show that our method maintains strong anthropomorphic features while ensuring accurate wrist pose tracking.**

I. Introduction

A. Motivation

Motion retargeting allows robots, particularly humanoid ones, to imitate human actions and acquire human skills efficiently. This approach is preferable to formulating specific policies for each task, as different tasks have unique requirements, making it impractical to define rules for all. While recent studies have explored teaching robots manipulation skills through learning algorithms [1, 2, 3, 4], motion retargeting has emerged as a crucial tool for skill acquisition.

B. Related Work

Off-line Motion Retargeting. Researchers have used optimization-based methods for offline motion retargeting in both single robot arms [5] and entire humanoid bodies [6]. Recently, learning-based approaches that generate anthropomorphic robot trajectories using latent space concepts have gained popularity [7, 8, 9]. However, offline motion retargeting faces challenges in scenarios requiring immediate feedback, such as robot-environment interactions, because the demonstrator cannot predict the interaction outcomes before executing the trajectory.

Real-time Whole-Body Motion Retargeting. Various methods have been developed for real-time motion retargeting of humanoid robots, primarily using optimization-based approaches for whole-body motion mapping [10, 11, 12, 13, 14]. Stanton et al. proposed a learning-based method for this purpose [15]. However, due to the complexity of managing many degrees of freedom (DOFs) in real-time whole-body retargeting, the control of the robot arms often lacks precision, leading to issues like poorly constrained end-effector orientation [10, 11, 12, 15] or unnatural arm vibrations [10, 13], which can impair the accuracy of the robot's arm control.

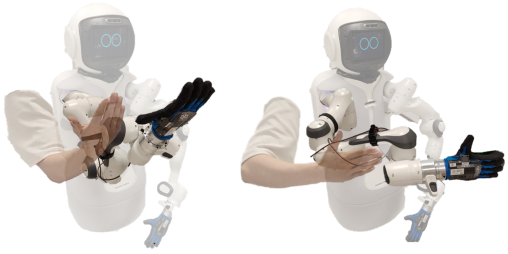

Fig. 1. Anthropomorphic arm mapping from human to humanoid robot.

Real-time Arm Motion Retargeting. As illustrated in Fig. 1, achieving anthropomorphic mapping from a human arm to a robot arm involves replicating the entire arm's pose. Most research on human-like robot arm motion focuses on Spherical-Rotational-Spherical (SRS) structured robots, as the SRS structure allows for the analytical solution of IK problems [16, 17, 18, 19]. However, many humanoid robots, such as ABB YuMi, Rethink Baxter, and Franka Emika Panda, do not conform to the SRS structure. To address this, Li et al. [20] proposed a real-time explicit mapping and teleoperation control (REMTC) method for 7-DOF non-SRS arms. The key idea of REMTC and its drawback will be described in subsection III-A. Given that optimization-based approaches have been successfully used for whole-body teleoperation, they could also be directly applied to real-time motion retargeting for non-SRS robot arms.

C. Contribution

In this paper, we introduce Optimization-Based Real-time Anthropomorphic Mapping (OBRAM). OBRAM imposes few restrictions on the robot arm's structure, making it suitable for arms with seven or more DOFs. We also introduce the use of the normalized normal vector of the arm plane as an anthropomorphic criterion within OBRAM.

To validate the proposed OBRAM method, we conducted extensive experiments, comparing OBRAM's performance with that of the Pose Tracking (PT) solver and REMTC. While some of the previous studies have evaluated wrist position accuracy [10, 6] or joint configuration accuracy [15, 9], most evaluations of motion retargeting present trajectory figures without providing comprehensive statistical analysis of accuracy and anthropomorphic indices. To address this gap, our evaluation includes detailed statistical analysis of both accuracy and anthropomorphic indices.

[1]All the authors are with the Munich Institute of Robotics and Machine Intelligence, Technical University of Munich, 80992 München, Germany. E-mails: {jimmy.yang, s.bien, simone.nertinger, djallil.naceri, haddadin}@tum.de.

We gratefully acknowledge the funding of the Lighthouse Initiative Geriatronics by StMWi Bayern (Project X, grant no. IUK-1807-0007// IUK582/001) and the funding of the Lighthouse Initiative Geriatronics by LongLeif GaPa gGmbH (Project Y).

† Corresponding Author

II. Optimization-Based Real-Time Arm Motion Anthropomorphic Mapping

This section introduces the framework of OBRAM, which enables real-time mapping of human arm motion to a robot arm. The general pipeline of OBRAM is depicted in Fig. 2.

A. Formulation of the Problem

Real-time motion mapping requires continuous input and output. The input consists of the human arm pose $\boldsymbol{p_{arm}}$, which includes the wrist pose as well as essential pose information from the shoulder and elbow. The output is the joint configuration $\boldsymbol{q}$ of the robot arm. An impedance controller can be used to convert $\boldsymbol{q}$ into motor torque, allowing for precise control of the robot arm. The mapping scheme, denoted as T_{map}, defines the relationship between $\boldsymbol{p_{arm}}$ and $\boldsymbol{q}$. To ensure both accurate tracking of the human wrist pose with the robot wrist and adherence to anthropomorphic principles, the mapping must satisfy constraints C_f related to the robot wrist pose p_{rw} and constraints C_a derived from anthropomorphic criteria. Thus, the mapping can be formulated as:

$$\boldsymbol{q} = T_{map}(\boldsymbol{p_{arm}}) \ subject\ to \begin{cases} C_f \leqslant \epsilon_f \\ C_a \leqslant \epsilon_a \\ \boldsymbol{q} \in (\boldsymbol{q_{min}}, \boldsymbol{q_{max}}) \end{cases} \tag{1}$$

where $\boldsymbol{q_{min}}$ and $\boldsymbol{q_{max}}$ are lower and higher limit of $\boldsymbol{p_{arm}}$, ϵ_f and ϵ_a are tolerance of C_f and C_a respectively. Our goal is to find out T_{map}.

B. Optimization-based Mapping Scheme

To mitigate the computational speed disadvantage of numerical IK, OBRAM avoids using methods that resolve redundancy through the null-space of IK [17]. Instead, OBRAM simultaneously solves IK while adhering to the anthropomorphic criterion, directly searching for a single solution that meets both functional and anthropomorphic requirements. As a result, the objective function $\boldsymbol{O}$ consisting of functional part $\boldsymbol{O}_f$ and anthropomorphic part $\boldsymbol{O}_a$ is defined as:

$$\begin{aligned} \boldsymbol{O}(\boldsymbol{p_{arm}}, \boldsymbol{q}) &= \left[\boldsymbol{O}_f, \boldsymbol{O}_a\right]^T, with \\ \boldsymbol{O}_f(\boldsymbol{p_{arm}}, \boldsymbol{q}) &= \left[w_f^1 O_f^1, \cdots, w_f^{n_p} O_f^{n_f}\right] \\ \boldsymbol{O}_a(\boldsymbol{p_{arm}}, \boldsymbol{q}) &= \left[w_a^1 O_a^1, \cdots, w_a^{n_a} O_a^{n_a}\right] \end{aligned} \tag{2}$$

where $O_f^i (i = 1, 2, ...n_f)$ and $O_a^j (j = 1, 2, ...n_a)$ are objective functions concerning functional and anthropomorphic constraints while $w_f^i (i = 1, 2, ...n_p)$ and $w_a^j (j = 1, 2, ...n_a)$ are weights. By minimizing the elements within $\boldsymbol{O}$ in parallel, the strictness of different constraints can be controlled by adjusting the corresponding weights. Lower weights make it easier to find solutions, while larger weights allow for more accurate control but increase the risk of non-convergence. Therefore, the weights can be fine-tuned as needed.

With the objective function, the optimization-based mapping scheme can be concluded as:

$$\boldsymbol{q} = \underset{\hat{\boldsymbol{q}}}{\operatorname{argmin}}(\boldsymbol{O}(\boldsymbol{p_{arm}}, \hat{\boldsymbol{q}})) \ with\ \hat{\boldsymbol{q}} \in (\boldsymbol{q_{min}}, \boldsymbol{q_{max}}) \tag{3}$$

where $\hat{\boldsymbol{q}}$ stands for joint configuration in the optimization process.

We adopt Trust Region Reflective (TRF) algorithm to solve this optimization problem because TRF can deal with bounds and behaves robustly in general [21].

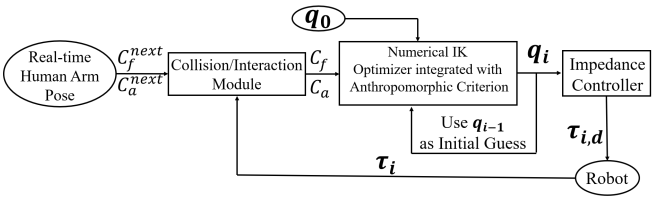

Fig. 2. Pipeline of OBRAM. $\boldsymbol{q_0}$ stands for the first initial guess that needs to be defined manually. C_f^{next} and C_a^{next} are functional and anthropomorphic constraint obtained from the arm pose respectively, while they will be determined as C_f and C_a after the Collision/Interaction Module. $\boldsymbol{q_i}$ is the current obtained joint configuration while $\boldsymbol{q_{i-1}}$ is the previous joint configuration. $\boldsymbol{\tau_{i,d}}$ is the desired joint torque array while $\boldsymbol{\tau_i}$ is the joint torque array observed by sensors.

C. Objective Function and Anthropomorphic Criterion

The objective function related to the pose constraint can be defined as the square error of the wrist pose, which is characterized by the orientation matrix $\boldsymbol{R_{rw}}$ and the position vector $\boldsymbol{p_{rw}}$. Therefore, each component of the functional part O_f^i corresponds to the square errors of the elements in $\boldsymbol{R_{rw}}$ and $\boldsymbol{p_{rw}}$.

Swivel angle Ψ [17] (as defined in Fig. 3(a)) and "Included Angle Minimization" (IAM) [20] are effective anthropomorphic criteria for SRS robot arms, as they can be integrated into the analytical IK process without requiring scaling, unlike distance-related criteria [22]. However, these criteria are not suitable for an optimization-based mapping scheme. The computation of swivel angle or included angle introduces unnecessary non-linearity, which complicates the optimization process.

Therefore, we propose the normalized normal vector of the arm plane illustrated in Fig. 3(b) as the anthropomorphic criterion. Compared with the swivel angle, which requires the computation of unit normal vectors for two planes and the inverse cosine function of their dot product, $\boldsymbol{n_{arm}}$ can represent the orientation of the arm plane with less computational cost and reduced non-linearity by only computing one unit vector:

$$\boldsymbol{n_{arm}} = \frac{\boldsymbol{v_{se}} \times \boldsymbol{v_{ew}}}{||\boldsymbol{v_{se}} \times \boldsymbol{v_{ew}}||} \tag{4}$$

where $\boldsymbol{v_{se}}$ is the shoulder-elbow vector and $\boldsymbol{v_{ew}}$ is the elbow-wrist vector. Normalization is needed to eliminate the influence from unit.

With the proposed anthropomorphic criterion, the corresponding objective functions O_a^j can be defined as the square errors of elements in $\boldsymbol{n_{arm}}$.

D. Scaling of Wrist Position

Due to the difference in length between the human and robot arms, it is necessary to scale the position of the human wrist to fit the robot's task space. The scaled position then becomes the desired position for the robot's wrist.

Typically, the wrist cannot reach the shoulder, even when the elbow is fully retracted. Therefore, we define a Spherical

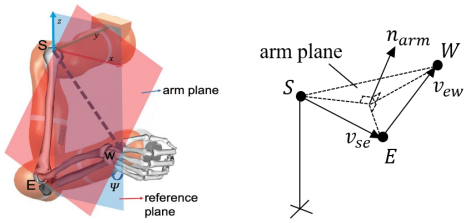

(a) Swivel angle Ψ [23]. (b) Normalized normal vector of arm plane $\boldsymbol{n_{arm}}$.

Fig. 3. Two anthropomorphic criteria: (a) swivel angle and (b) normalized normal vector of arm plane. S, E and W represent shoulder, elbow and wrist separately.

Shell Task Space (SSTS) for the human arm, as shown in the longitudinal section in Fig. 4. Similarly, an SSTS is defined for the robot arm. Both human and robot arms are constrained by their joint limits within their respective SSTS. Our goal is to map the position in the human SSTS Ω_H into the Robot SSTS Ω_R.

We adopt linear mapping to address this problem. Given $l_{max,h}$ and $l_{max,r}$ as the lengths of the human and robot arms, respectively, and $l_{min,h}$ and $l_{min,r}$ as the minimum distances from the shoulder to the wrist for the human and robot, the position scaling factor can be expressed as:

$$k_p = \frac{l_{max,r} - l_{min,r}}{l_{max,h} - l_{min,h}} \tag{5}$$

The desired position vector pointing from robot shoulder to wrist $\boldsymbol{p_{sw,r}}$ can be then obtained by:

$$\boldsymbol{p_{sw,r}} = [k_p(||\boldsymbol{p_{sw,h}}|| - l_{min,h}) + l_{min,r}]\boldsymbol{u_{sw,h}} \tag{6}$$

where $||\boldsymbol{p_{sw,h}}||$ represents the length between human shoulder and wrist while $\boldsymbol{u_{sw,h}}$ is the unit vector pointing from human shoulder to wrist.

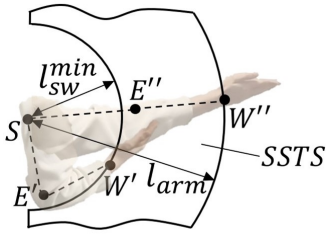

Fig. 4. Longitudinal section of Spherical Shell Task Space (SSTS). S represents shoulder. E' and W' are elbow and wrist when the elbow is retracted at extreme position. E'' and W'' are elbow and wrist when the elbow is extended at extreme position. l_{sw}^{min} is the minimum distance between shoulder and wrist while l_{arm} is the length of arm.

III. Validation and Discussion

In this section, we first review REMTC [20] and present a general approach to replicate its performance. Since REMTC was developed for non-SRS robot arms, comparing OBRAM with REMTC is pertinent. We evaluate OBRAM's performance in terms of both functional and anthropomorphic aspects, assessing static and dynamic behaviors. PT, focusing solely on the wrist pose, is used as the upper limit benchmark for wrist pose accuracy. We compare the anthropomorphic features of OBRAM with those of REMTC and also test OBRAM's capability to handle pose limits and interactions with humans.

Wrist pose accuracy serves as the index for functional performance, while the swivel angle, as used in many studies [14, 17, 23, 24], is the primary index for anthropomorphic performance. The normalized normal vector of the arm plane ($\boldsymbol{n_{arm}}$) is evaluated as an auxiliary anthropomorphic index. The position error e_{pos} is defined as the absolute distance between the desired and actual wrist positions. The orientation error e_o is defined as:

$$e_o = \frac{e_{ox} + e_{oy} + e_{oz}}{3} \tag{7}$$

where e_{ox}, e_{oy} and e_{oz} are the angles between the corresponding axes of desired and actual wrist frame. The error of swivel angle e_{sa} is defined as the absolute difference between desired and actual swivel angle. e_{nnv}, the error of $\boldsymbol{n_{arm}}$, is the angle between the desired and actual $\boldsymbol{n_{arm}}$.

We used Vicon's optical motion capture system to record human motion. The inputs include the human wrist and shoulder poses, as well as the elbow position, with the wrist pose relative to the shoulder frame being the desired output. Other sensors may be used, provided they can capture the same input pose data.

The experiments were conducted on GARMI robot, which features two 7-DOF Franka Emika Panda arms (DH parameters listed in Table I). DH parameters in parentheses indicate parameters for a similar SRS structure used in REMTC. The shoulder, elbow, and wrist joints of the robot were defined as follows: the 1st joint as the shoulder, the 4th joint as the elbow, and the 7th joint as the wrist. The solving process was executed on an Intel NUC7i7BNH with an Intel Core i7-7567U CPU @ 3.50GHz.

TABLE I

DH Table of Franka Emika Panda

joint	α/rad	a/m	d/m	θ/rad
1	0	0	0.333	θ_1
2	$-\pi/2$	0	0	θ_2
3	$\pi/2$	0	0.316	θ_3
4	$\pi/2$	0.0825 (0)	0	θ_4
5	$-\pi/2$	-0.0825 (0)	0.384 (0.394)	θ_5
6	$\pi/2$	0	0	θ_6
7	$\pi/2$	0.088 (0)	0 (0.098)	θ_7

A. Performance Replication and Discussion of REMTC

The workflow of REMTC for non-SRS robot arm is summarized as follows: (1) Transform the robot structure into a similar SRS structure; (2) Solve IK analytically using anthropomorphic constraints with the SRS structure; (3) Take the solution obtained in the previous step as initial guess for numerical IK that only considers functional constraint.

The analytical IK methods proposed by Li et al. [20] and Shimizu et al. [17] face limitations: their methods use less than six DOFs for determining end-effector pose, whereas six DOFs are theoretically required. A generic approach to replicate solution of different types of analytical IK is to use a constraint-reduced numerical process. In this study, we use seven out of nine entries from the wrist's orientation matrix and its full position array as functional constraints in the numerical process. The normalized normal vector ($\boldsymbol{n_{arm}}$) serves as an anthropomorphic constraint. To ensure fast resolution, solutions from this numerical process are

precomputed for each trajectory and used in the final step of REMTC to actuate the robot's execution.

The core concept of REMTC is to incorporate anthropomorphic features into the initial guess from analytical IK, and then satisfy the functional constraints in the final numerical solution. However, the omission of anthropomorphic constraints in the final numerical step can lead to jitters. Such jitters are evident in the video attached in [20] and observed in the dynamic evaluation of this study.

B. Static Performance

In the static evaluation, the robot was positioned in the same 19 poses using PT, REMTC, and OBRAM for comparison. Indices for each method were collected at each pose and are presented in Fig. 5.

Fig. 5(a) and 5(b) display the pose errors. Table II provides the mean absolute error (MAE) and standard deviation (SD) for wrist position and orientation using PT, REMTC, and OBRAM. A T-Test was conducted to compare the functional performance of REMTC and OBRAM against PT as a benchmark. For position, REMTC demonstrated a confidence level of approximately 99% that its position error is no more than 1 mm greater than PT's, while OBRAM achieved a 95% confidence level for the same threshold. For orientation, both REMTC and OBRAM were affirmed to have errors no more than 0.5° greater than PT with a confidence level exceeding 99%. These results suggest that the anthropomorphic attributes of REMTC and OBRAM do not likely to compromise their functional performance for tasks requiring wrist position and orientation accuracy within 1 cm and 2°.

Fig. 5(c) and 5(d) illustrate the anthropomorphic features of PT, REMTC, and OBRAM. PT, which does not account for anthropomorphism, shows substantial errors in anthropomorphic indices. Table II provides the MAE and SD for swivel angle and $\boldsymbol{n_{arm}}$. While REMTC performs better than PT, its MAE for swivel angle (10.96°) and $\boldsymbol{n_{arm}}$ (10.75°) remains above 10°, whereas OBRAM achieves MAEs of 0.47° and 0.94° respectively, both below 1°. The T-Test results indicate that, with over 95% confidence, OBRAM's swivel angle error is 7° less than REMTC's, confirming that the anthropomorphic feature is diminished in the final step of REMTC. In contrast, OBRAM maintains superior anthropomorphic features.

TABLE II

BASIC STATISTICAL ANALYSIS IN STATIC EVALUATION

		MAE	**SD**
Position/mm	PT	6.6	**2.1**
	REMTC	**5.5**	2.2
	OBRAM	6.2	3.2
Orientation/°	PT	**1.25**	0.44
	REMTC	1.32	0.47
	OBRAM	1.39	**0.39**
Swivel Angle/°	PT	85.61	39.86
	REMTC	10.96	5.66
	OBRAM	**0.47**	**0.53**
$\boldsymbol{n_{arm}}$/°	PT	84.35	38.73
	REMTC	10.75	5.57
	OBRAM	**0.94**	**0.25**

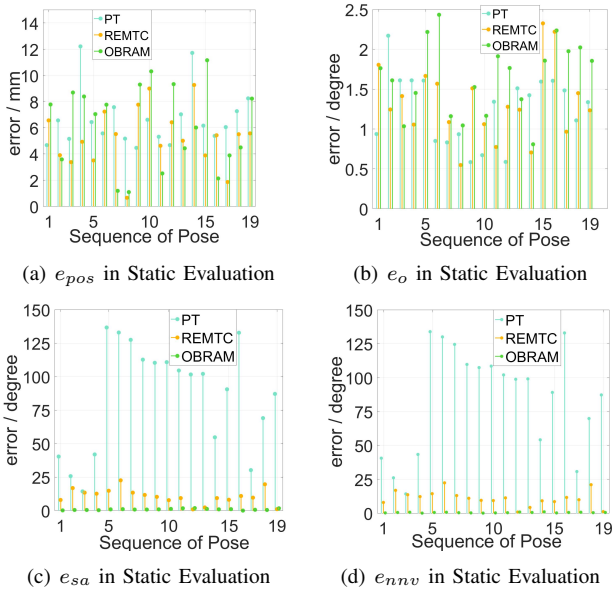

(a) e_{pos} in Static Evaluation (b) e_o in Static Evaluation

(c) e_{sa} in Static Evaluation (d) e_{nnv} in Static Evaluation

Fig. 5. Static errors of PT, REMTC and OBRAM.

C. Dynamic Performance

In the dynamic assessment, the robot arm executed three types of trajectories: swiveling, abduction, and picking. Fig. 6 shows the mean errors for each trajectory type. Additionally, example gestures mapped from the human arm to the robot arm are presented in Fig. 8. The MAEs of the evaluation indices employing PT, REMTC and OBRAM are presented in Fig. 6.

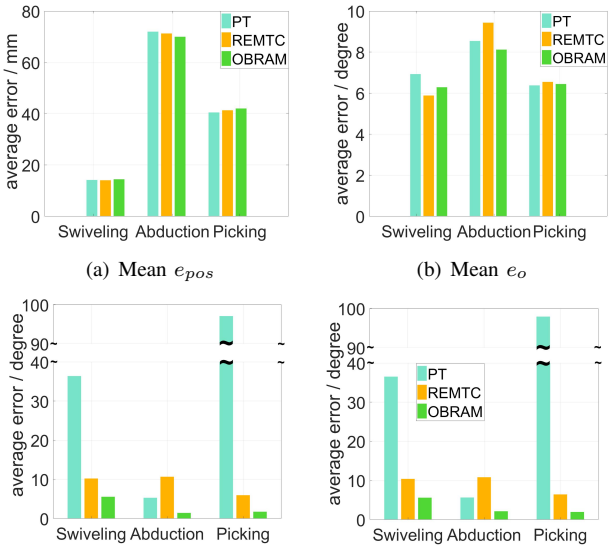

(a) Mean e_{pos} (b) Mean e_o

(c) Mean e_{sa} (d) Mean e_{nnv}

Fig. 6. MAE of PT, REMTC and OBRAM in three trajectories.

Table III lists the average resolution frequencies for the three methods. The table shows that PT and REMTC are faster than OBRAM, as OBRAM involves solving an optimization problem with more constraints. Despite this, OBRAM does not exhibit any decline in trajectory smoothness and even demonstrates superior dynamic performance compared to REMTC, as in the following discussion.

Fig. 7 illustrates the picking trajectory in the dynamic

evaluation. The charts depict the x position of the robot wrist and the swivel angle for the corresponding trajectories. Both REMTC and OBRAM can track the desired wrist pose similarly to PT; however, OBRAM maintains a swivel angle closest to the desired value. The swivel angle curves reveals jagged segments in REMTC's trajectory, indicative of jitters. Such jittering is not present in the x position trajectory, suggesting that the resolution frequency is not the cause. Instead, the loose anthropomorphic constraint in REMTC's final step likely contributes to these jitters. In contrast, OBRAM ensures a smooth trajectory throughout the movement.

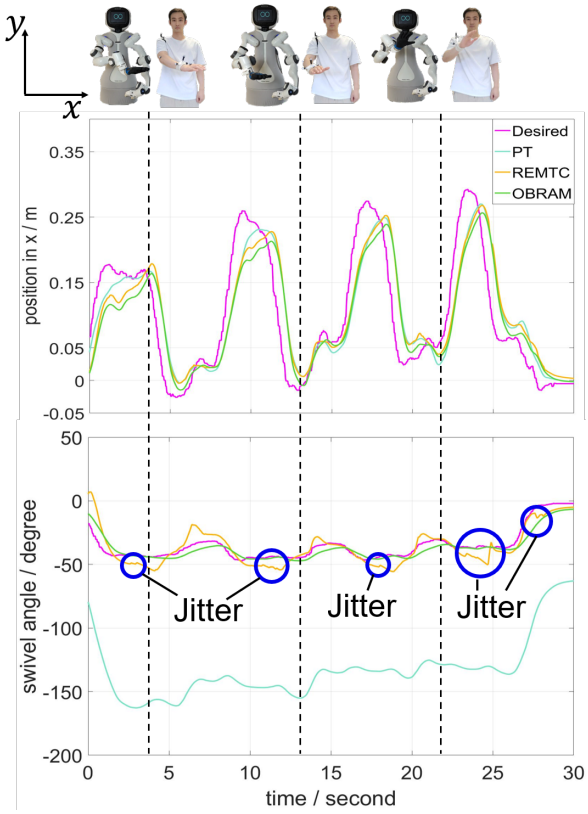

Fig. 7. Robot wrist picking trajectory in x direction and swivel angle in picking trajectory.

TABLE III

AVERAGE RESOLUTION FREQUENCY

	PT	REMTC	OBRAM
frequency / Hz	97.09	74.07	38.46

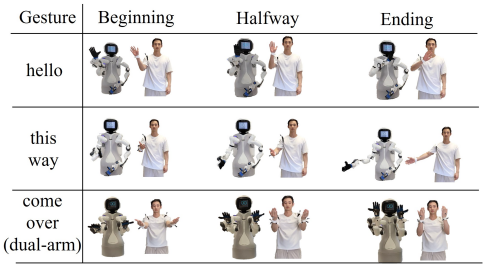

Fig. 8. Example gestures mapping from human to robot with OBRAM.

D. Discussion on Anthropomorphic Criterion

The static and dynamic evaluations (Fig. 5(c) and 5(d), Fig. 6(c) and 6(d)) reveal that the behaviors of swivel angle and $\boldsymbol{n_{arm}}$ are highly similar. The Pearson correlation coefficient r between the errors of swivel angle and $\boldsymbol{n_{arm}}$ is 0.9998, indicating a strong linear correlation. This correlation is due to both criteria being related to the orientation of the arm plane. The IAM criterion proposed by Li et al. [20] also reflects this concept, emphasizing the orientation of the arm plane as a practical standard for anthropomorphism in robot arm control. While the orientation of the arm plane serves as a useful anthropomorphic feature, selecting or designing appropriate criteria for specific methods is essential.

E. Task Space Limit

Since the robot arm differs structurally from the human arm, their task spaces have different limits. In OBRAM, when the robot arm's joints reach their limits, the arm remains at this limit pose. The robot arm will continue tracking the desired pose once an applicable solution is available. Fig. 9 illustrates three examples of both human and robot arms attempting to reach certain limit poses.

(a) (b) (c)

Fig. 9. Examples of joints limits.

F. Feasibility of Collision/Interaction Module

We conducted an interaction test between the robot and a human to simulate rehabilitation and assess the feasibility of integrating a physical interaction model into OBRAM. During the test, a human hand restrained GARMI's hand from translating or rotating in the real-time motion retargeting experiment. Despite the robot hand maintaining its pose, the rest of the arm was still able to move within the null space. GARMI's hand could be reactivated when it attempted to move alongside the applied force or moment. Fig. 10 provides a demonstration of this interaction process.

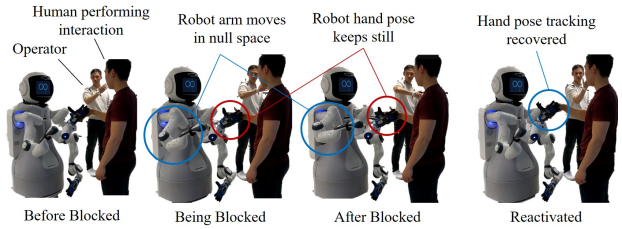

Fig. 10. Demonstration of interaction.

IV. CONCLUSION AND FUTURE WORK

This paper studies an optimization-based real-time anthropomorphic mapping (OBRAM) for transferring human arm motion to a robot arm. The scheme is simple but efficient, applicable to SRS and non-SRS robot arms for real-time motion retargeting. Experimental results and statistical analysis demonstrate that OBRAM tracks human wrist pose with accuracy comparable to PT, while offering superior anthropomorphic features compared to REMTC.

The study's limitations include validation being restricted to GARMI, suggesting the need for future tests on additional robot arm types. Further research could focus on enabling humanoid robots to generate human-like motion autonomously,

leveraging the anthropomorphic features learned through OBRAM.

REFERENCES

[1] Tony Z Zhao et al. "Learning fine-grained bimanual manipulation with low-cost hardware". In: *arXiv preprint arXiv:2304.13705* (2023).

[2] Eric Jang et al. "Bc-z: Zero-shot task generalization with robotic imitation learning". In: *Conference on Robot Learning*. PMLR. 2022, pp. 991–1002.

[3] Anthony Brohan et al. "RT-1: Robotics Transformer for Real-World Control at Scale". In: *arXiv e-prints* (2022), arXiv–2212.

[4] Ajay Mandlekar et al. "What matters in learning from offline human demonstrations for robot manipulation". In: *arXiv preprint arXiv:2108.03298* (2021).

[5] Guilherme Maeda et al. "Acquiring and generalizing the embodiment mapping from human observations to robot skills". In: *IEEE Robotics and Automation Letters* 1.2 (2016), pp. 784–791.

[6] Ko Ayusawa and Eiichi Yoshida. "Motion retargeting for humanoid robots based on simultaneous morphing parameter identification and motion optimization". In: *IEEE Transactions on Robotics* 33.6 (2017), pp. 1343–1357.

[7] Sungjoon Choi and Joohyung Kim. "Towards a natural motion generator: A pipeline to control a humanoid based on motion data". In: *2019 IEEE/RSJ International Conference on Intelligent Robots and Systems (IROS)*. IEEE. 2019, pp. 4373–4380.

[8] Haodong Zhang et al. "Kinematic motion retargeting via neural latent optimization for learning sign language". In: *IEEE Robotics and Automation Letters* 7.2 (2022), pp. 4582–4589.

[9] Yashuai Yan, Esteve Valls Mascaro, and Dongheui Lee. "ImitationNet: Unsupervised Human-to-Robot Motion Retargeting via Shared Latent Space". In: *2023 IEEE-RAS 22nd International Conference on Humanoid Robots (Humanoids)*. IEEE. 2023, pp. 1–8.

[10] Jonas Koenemann, Felix Burget, and Maren Bennewitz. "Real-time imitation of human whole-body motions by humanoids". In: *2014 IEEE International Conference on Robotics and Automation (ICRA)*. IEEE. 2014, pp. 2806–2812.

[11] Alessandro Di Fava et al. "Multi-contact motion retargeting from human to humanoid robot". In: *2016 IEEE-RAS 16th international conference on humanoid robots (humanoids)*. IEEE. 2016, pp. 1081–1086.

[12] Luigi Penco et al. "Robust real-time whole-body motion retargeting from human to humanoid". In: *2018 IEEE-RAS 18th International Conference on Humanoid Robots (Humanoids)*. IEEE. 2018, pp. 425–432.

[13] Kourosh Darvish et al. "Whole-body geometric retargeting for humanoid robots". In: *2019 IEEE-RAS 19th International Conference on Humanoid Robots (Humanoids)*. IEEE. 2019, pp. 679–686.

[14] Hang Su et al. "An incremental learning framework for human-like redundancy optimization of anthropomorphic manipulators". In: *IEEE Transactions on Industrial Informatics* 18.3 (2020), pp. 1864–1872.

[15] Christopher Stanton, Anton Bogdanovych, and Edward Ratanasena. "Teleoperation of a humanoid robot using full-body motion capture, example movements, and machine learning". In: *Proc. Australasian Conference on Robotics and Automation*. Vol. 8. 2012, p. 51.

[16] Tamim Asfour and Rüdiger Dillmann. "Human-like motion of a humanoid robot arm based on a closed-form solution of the inverse kinematics problem". In: *Proceedings 2003 IEEE/RSJ International Conference on Intelligent Robots and Systems (IROS 2003)(Cat. No. 03CH37453)*. Vol. 2. IEEE. 2003, pp. 1407–1412.

[17] Masayuki Shimizu et al. "Analytical inverse kinematic computation for 7-DOF redundant manipulators with joint limits and its application to redundancy resolution". In: *IEEE Transactions on robotics* 24.5 (2008), pp. 1131–1142.

[18] Weihui Liu, Diansheng Chen, and Jochen Steil. "Analytical inverse kinematics solver for anthropomorphic 7-DOF redundant manipulators with human-like configuration constraints". In: *Journal of Intelligent & Robotic Systems* 86 (2017), pp. 63–79.

[19] Isiah Zaplana, Hugo Hadfield, and Joan Lasenby. "Closed-form solutions for the inverse kinematics of serial robots using conformal geometric algebra". In: *Mechanism and Machine Theory* 173 (2022), p. 104835.

[20] Shengjie Li et al. "A real-time explicit mapping and teleoperation control method for humanoid robots with posture constraints". In: *Mechatronics* 90 (2023), p. 102937.

[21] Mary Ann Branch, Thomas F Coleman, and Yuying Li. "A subspace, interior, and conjugate gradient method for large-scale bound-constrained minimization problems". In: *SIAM Journal on Scientific Computing* 21.1 (1999), pp. 1–23.

[22] Minas V Liarokapis et al. "Directions, methods and metrics for mapping human to robot motion with functional anthropomorphism: A review". In: *School of Mechanical Engineering, National Technical University of Athens, Tech. Rep* (2013).

[23] Hang Su et al. "Deep neural network approach in human-like redundancy optimization for anthropomorphic manipulators". In: *IEEE Access* 7 (2019), pp. 124207–124216.

[24] Cecilia Lamperti, Andrea Maria Zanchettin, and Paolo Rocco. "A redundancy resolution method for an anthropomorphic dual-arm manipulator based on a musculoskeletal criterion". In: *2015 IEEE/RSJ International Conference on Intelligent Robots and Systems (IROS)*. IEEE. 2015, pp. 1846–1851.